Applied Surface Science 563 (2021) 150364

Contents lists available at ScienceDirect

Applied Surface Science

journal homepage: www.elsevier.com/locate/apsusc

Full Length Article

Effect of hydrogen peroxide on bovine serum albumin adsorption on Ti6Al4V alloy: A scanning Kelvin probe force microscopy study

Ehsan Rahimi [a], Ruben Offoiach [a], Saman Hosseinpour [b,c], Ali Davoodi [c], Kitty Baert [d], Alexander Lutz [d], Herman Terryn [d], Maria Lekka [a,e,*], Lorenzo Fedrizzi [a]

[a] Polytechnic Department of Engineering and Architecture, University of Udine, 33100 Udine, Italy
[b] Institute of Particle Technology (LFG), Friedrich-Alexander-Universität-Erlangen-Nürnberg (FAU), Cauerstraße 4, 91058 Erlangen, Germany
[c] Materials and Metallurgical Engineering Department, Faculty of Engineering, Ferdowsi University of Mashhad, Mashhad 91775-1111, Iran
[d] Vrije Universiteit Brussel, Department of Materials and Chemistry, Research Group Electrochemical and Surface Engineering, Pleinlaan 2, 1050 Brussels, Belgium
[e] CIDETEC, Basque Research and Technology Alliance (BRTA), Po. Miramón 196, 20014 DonostiaSan Sebastián, Spain

ARTICLE INFO

Keywords:
Hydrogen peroxide
Albumin protein
Ti6Al4V alloy
Protein surface potential
SKPFM

ABSTRACT

Protein adsorption on the surface of implant materials greatly affects the performance of the implants, such as their stability as well as the release of metal ions from and the adhesion of cells to their surface. In addition, the production of extracellular H_2O_2 from the activation of inflammatory cells could interfere with protein–metal interactions and/or modify the conformation of adsorbed proteins. In this study, we utilised scanning Kelvin probe force microscopy (SKPFM) to visualise the impact of H_2O_2 on bovine serum albumin (BSA) adsorption on the positively polarised Ti6Al4V alloy in a phosphate-buffered saline (PBS) solution. We show that the negatively charged BSA adsorbs onto the surface of polished and anodically polarised Ti6Al4V in a dense layer with a continuous network-like morphology or cluster shape and reduces the variation in the total surface potential compared to that of blank Ti6Al4V. However, addition of H_2O_2 to the PBS solution interferes with the formation of the dense protein network, and only a thin and discontinuous protein layer adsorbs onto the surface of the Ti6Al4V alloy, lowering the total surface potential difference. The information presented in this work provides new insights into the adsorption distribution of proteins on metallic substrates in biomaterials field.

1. Introduction

The tissue compatibility and cell adhesion properties of implants are primarily affected by the interactions of proteins during the implantation of biomaterials in the human body [1,2]. The amount of protein that is adsorbed, its type, and its conformational arrangement strongly control subsequent interactions, including adhesion and proliferation of the cell, inflammatory responses, and particularly metal-ion release from the solid surface (i.e. degradation processes) [3]. Protein adsorption on solid surfaces is a complex process involving electrostatic, hydrophobic, and van der Waals interactions as well as hydrogen bonding [3,4]. According to previous reports [5,6], the electrostatic and hydrophobic interactions are greatly influenced by the surface properties of the substrate as well as the physiological conditions (e.g. pH, ion concentration, and temperature).

Titanium and titanium alloys are among the most widely used biomaterials owing to their biocompatibility, excellent mechanical properties, and high corrosion resistance [7]. Thus far, titanium alloys have been used in orthopaedic, dental and cardiovascular devices, the main implants that replace hard tissue [8]. Ti6Al4V alloy is one of the most well-known titanium alloys because it combines high corrosion resistance and excellent mechanical properties due to its dual microstructure with mixed alpha (α) and beta (β) phases [9]. Nevertheless, after exposure to physiological media and upon interaction with proteins, inadequate osseointegration and osteoconductivity as well as increased metal-ion release have been reported for these materials [7,10]. Cathodic and anodic electrochemical reactions on the oxide film of titanium and its alloys in physiological media lead to the reduction of oxygen, which proceeds through partial reactions with radicals and hydrogen peroxide (H_2O_2) [11,12]. Moreover, the activation of inflammatory cells, particularly macrophages and neutrophils (which are the first cells that adsorb onto the implant surface), trigger the production of high amounts (i.e. μM-mM) of reactive oxygen species (ROS) and extracellular H_2O_2 [10,12]. The presence of ROS and H_2O_2 further

* Corresponding author at: CIDETEC, Basque Research and Technology Alliance (BRTA), Po. Miramón 196, 20014 DonostiaSan Sebastián, Spain.
E-mail address: mlekka@cidetec.es (M. Lekka).

https://doi.org/10.1016/j.apsusc.2021.150364
Received 13 February 2021; Received in revised form 31 May 2021; Accepted 10 June 2021
Available online 15 June 2021

complicates the electrochemical reactions and metal-ion release at the oxide layer/protein interface [13]. Likewise, the interaction of H_2O_2 species with certain transition-metal ions can produce $HO^{\cdot}$ radicals in a Fenton-type reaction, which can oxidise organic compounds such as proteins and DNA [14,15].

Proteins are often considered to be electrically conductive substances, and their electrical conductivity (EC) after adsorption on a surface, which can be described as a homogeneous or heterogeneous metal–oxide hybrid, can alter electrochemical interactions and affect metal-ion release from the protein-covered surface [6,16]. The EC of protein molecules strongly depends on the composition of their amino acids as well as their molecular structure [17]. A large number of experimental methods have been utilised to study the conductivity of biological molecules, particularly proteins. These methods provide valuable in-situ and ex-situ insights with respect to the EC of adsorbed proteins on solid surfaces and include sandwiching proteins between two solid electrodes [18,19], scanning tunneling microscopy [20–24], conductive atomic force microscopy (C-AFM) [25–27], scanning Kelvin probe force microscopy (SKPFM) [28–30], and electrochemical measurements (cyclic voltammetry) [31,32]. For instance, Ron et al. showed that tryptophan residue results in high EC in Azurin and bacteriorhodopsin proteins [18]. Using C-AFM, Xu et al. showed that the EC of holoferritin and apoferritin is related to their conductive core as opposed to their more insulating shell [33]. In contrast, serum albumin protein is characterised by low EC [17,18], and thus its adsorption on metallic substrates can impede electrochemical reactions between the metal and electrolyte.

SKPFM enables the measurement of the electrical potential or surface charge distribution in various systems, including organic and inorganic thin films, micro-electronics, and biological samples, with high spatial and electrical resolution [34,35]. The concept of measuring the difference in the work function energy (*WFE*, ϕ) between two separate materials was originally established by Lord Kelvin [36], and Kelvin probe measurement techniques were further improved and developed by other researchers [37,38]. The surface potential is sensitive to any type of chemical variation, structural change, or surface defect and can be used to predict electrochemical activities [39–41]. Owing to its high lateral and potential resolution, SKPFM is able to detect charging and discharging processes in a single molecule [34] or to distinguish localised charges in biological systems, such as DNA and proteins [42]. In this study, we used SKPFM as a sensitive method to visualise the adsorption and distribution of bovine serum albumin (BSA) on the surface of anodically polarised Ti6Al4V. By combining SKPFM with scanning electron microscopy (SEM), in-situ atomic force microscopy (AFM), electrochemical measurements, and X-ray photoelectron spectroscopy (XPS), we determined the effect of H_2O_2 on the adsorption distribution of BSA on the heterogeneous surface of Ti6Al4V with α and β phases in the phosphate-buffered saline (PBS) solution.

2. Experimental procedure

2.1. Sample preparation

The specimens were cut from a bulk Ti6Al4V (ASTM F1472) alloy in the form of discs with a surface area of approximately 0.36 cm^2 and a thickness of 1 cm. The chemical composition (in wt.%) of the Ti6Al4V alloy was 6.25 Al, 0.065 C, 0.23 Fe, 0.003 H, 0.01 N, 0.185 O, 4.45 V, and 0.001 Y (balance Ti). The specimens were wet ground from #500 to #4000 mesh with SiC abrasive foil and then polished with an alumina slurry to achieve a mirror-like surface. Finally, the samples were cleaned in an acetone ultrasonic bath for 30 min and then washed with deionised water and dried by blowing air.

2.2. Electrolyte and electrochemical measurements

The PBS solution was prepared according to the ASTM Standard (F2129) [43] using 8 $g{\cdot}L^{-1}$ NaCl, 0.2 $g{\cdot}L^{-1}$ KCl, 1.15 $g{\cdot}L^{-1}$ Na_2HPO_4, 0.2 $g{\cdot}L^{-1}$ KH_2PO_4. Protein solutions with a concentration of 1 $g{\cdot}L^{-1}$ were prepared by adding lyophilized BSA powder (Sigma–Aldrich, ≥96% agarose gel electrophoresis) to the PBS solution. The pH of the protein solutions was measured using a pH meter (GLP 21, CRISON) and was 7.4 ± 1 at 37 °C. To simulate harsh inflammation conditions in vitro, hydrogen peroxide (H_2O_2, PanReac Applichem, 30% w/v (100 vol)) with a concentration of 100 μM was added to the protein solution [44].

Electrochemical measurements (potentiostatic polarisation and potentiodynamic polarisation (PDP)) of the Ti6Al4V alloys were performed using an AUTOLAB PGSTAT 30 potentiostat instrument. An $Ag/AgCl/KCl_{3M}$ electrode (+222 mV vs. SHE) and a platinum wire were used as the reference and counter electrodes, respectively, and the Ti6Al4V specimen was used as the working electrode. The PDP measurements were conducted at a scan rate of 1 $mV{\cdot}s^{-1}$ from cathodic to anodic potentials after 1-hour immersion indifferent solutions, including in blank PBS, PBS + BSA, PBS + H_2O_2, and PBS + BSA + H_2O_2, to reach the steady-state condition and stabilised open-circuit potential (OCP). For AFM/SKPFM surface imaging, the working electrodes (Ti6Al4V) were anodically polarised at a constant potential of + 200 mV vs. Ag/AgCl for 1-hour in PBS, PBS + BSA or PBS + BSA + H_2O_2 solutions. After this process, all samples were rinsed with deionised water to remove weakly adsorbed species from their surface, which could influence the surface analysis results. All specimens were dried with blowing air and finally stored in a desiccator.

2.3. Microstructural characterisation and SPM measurements

To investigate the effect of adsorbed BSA as well as the role of H_2O_2 on the surface potential distribution of the Ti6Al4V alloys, combined SEM, in-situ AFM, and SKPFM measurements were performed. Surface examination was conducted using a field-emission scanning electron microscope (JEOL, JSM-7610FPlus, 5 kV, and a working distance of 15 mm) with a secondary electron (SE) detector. AFM/SKPFM mapping was performed to evaluate the topography and surface potential distribution on the Ti6Al4V specimen in the blank PBS solution and also with or without BSA and H_2O_2. A Digital Instruments Nanoscope IIIa Multimode scanning probe microscope (SPM) with n-type doped silicon pyramid single-crystal tip coated with PtIr5 (SCM-Pit probe, tip radius and height were 20 nm and 10–15 μm, respectively) was used for the AFM/SKPFM measurements. The surface potential maps were recorded in dual-scan mode. In the first scan, topography data were obtained in the dynamic mode (also known as tapping mode). In the second scan, the tip was raised to 100 nm, and the surface potential was recorded by following the topography contour registered in the first scan. Topography and surface potential maps were collected ex-situ in an air atmosphere at 27 °C and a relative humidity of approximately 28%. A pixel resolution of 512 × 512, a zero-bias voltage, and a scan frequency rate of 0.2 Hz were used in all AFM/SKPFM measurements. In-situ AFM maps in the electrolyte were recorded in contact mode using a Park AFM XE-100 instrument while the specimen was polarised to + 200 mV vs. Ag/AgCl in an electrolyte containing only PBS + BSA for 1-hour at 37 °C. Histogram and power spectral density (PSD) analyses based on the multimodal Gaussian distributions and fast Fourier transform, respectively, were used to interpret the topography and surface potential distribution on the heterogeneous surface. The analyses were performed following the procedure described in previous studies [45,46].

2.4. X-ray photoelectron spectroscopy (XPS)

Ex-situ XPS measurements were performed using a PHI-5000 Versaprobe II (Physical Electronics) with a monochromatic Al Kα X-ray source (1486.71 eV photon energy) and a spot diameter of 100 μm. The irradiation power of the X-ray beam was set to 25 W to avoid beam-induced damage of the protein-covered samples. The kinetic energy of the photoelectrons was measured with a take-off angle of 45°. The

vacuum in the analysis chamber was set to at least 1×10^{-9} Torr. The XPS spectra were analysed using the PHI Multipack software (V9.0). High-resolution scans of C 1s, N 1s, and Ti 2p were obtained with a pass energy of 23.5 eV and 0.05 eV energy step size.

3. Results and discussion

3.1. Influence of protein on energy level evaluations by SKPFM

Using a conductive probe with a low electron-transfer resistance in SKPFM/AFM measurements allows the local surface potential or *WFE* distribution on a substrate to be determined without any physical contact between the tip and surface [25]. Fig. 1**a** demonstrates the basic principle of SKPFM along with the energy levels (conduction and valence bands (E_{CB} and E_{VB}), Fermi level (E_f), and vacuum level (VL)) of the tip and substrate. The bare substrate is schematically represented as a bulk alloy covered with an oxide layer. The electrostatic interactions between the scanning tip and the sample surface depend on the EC of the substrate and the bias voltage (positive and negative bias voltage) applied to the tip as well as the tip–sample distance [25].

The local surface potential is fundamentally affected by the surface or bulk charges, surface dipoles, and density of surface electronic states [35]. Therefore, at a constant bias voltage and tip–sample distance, the recorded *WFE* values can correspond to the local surface potential difference (ΔSP) between the probe and the studied substrate [34]:

$$\Delta SP = (\varnothing_p - \varnothing_s)/e \quad (1)$$

where e is the elementary charge, and $\varnothing_p$ and $\varnothing_s$ are the *WFE* of the probe and substrate, respectively. In a simple semiconductor or dielectric material, the surface potential strongly correlates with the surface charge [42]. In a more complex system, such as the Ti6Al4V alloy with a heterogeneous distribution of oxide compounds, the recorded surface potential represents the concentration-weighted sum of the *WFEs* of the oxide constituents, in this case as $WFE_{total} = \varnothing_{p\mathrm{TiO2}} + \varnothing_{p\mathrm{Al2O3}} + \varnothing_{p\mathrm{V2O3}}$ [47]. Likewise, phases with different chemical compositions within an alloy exhibit different WFE_{total}. The microstructure of a Ti6Al4V alloy is composed of two individual phases, α and β, with different chemical compositions (the α and β phases are visualised in the SEM micrographs in Fig. 2). Thus, in Ti6Al4V, the nominal *WFE* of the α (86.0% Ti, 2.0 % V, and 12.0% Al) and β (79.5% Ti, 12.2 % V, and 8.3% Al) phases can be estimated using the following equation [48]:

$$WFE = \frac{\sum_i W_i \times a_i}{\sum_i a_i} \quad (2)$$

where W_i is the work function of the individual element i, and a_i is its atomic percentage. The *WFE* of Ti, Al, and V in the polycrystalline condition are ~ 4.33, ~4.24, and ~ 4.3 eV, respectively [49]. Based on the content (i.e. atomic percentage) of these elements in the α and β phases, their corresponding *WFEs* can be calculated, as presented in Table 1.

Furthermore, the semiconducting characteristics of the surface layer (e.g. n- or p-type, bandgap, position of occupied and unoccupied states, oxygen vacancies, cation interstitials, etc.) affect the magnitude of the surface potential. For example, in the Ti6Al4V metallic alloy, TiO_2 and Al_2O_3 are n-type semiconductors with a wide bandgap, and V_2O_3 exhibits defective semiconductor properties [50]. The different surface charge states of the oxide layers on the α and β phases can influence the adsorption distribution of BSA [51,52].

It has been previously demonstrated that the adsorption of a monolayer or a multilayer of organic molecules, such as chemisorbed self-assembled monolayers (SAMs), Langmuir–Blodgett (LB) films, and even single proteins, influence the measured surface potential (SP_{Oxide}) [35,53], as schematically represented in Fig. 1**b** for the BSA molecules on the surface. As shown in this figure, adsorbed BSA molecules on the surface oxide affect the surface energy levels and influence the electrostatic interaction between the tip and BSA-covered oxide layer. The BSA–oxide layer interaction also induces band bending (V_{bb}) and alters the effective molecular dipole (μ_{BSA}) and interface dipole (Δ_{bond}), as shown in Fig. 1**b**. These changes in the surface energy levels originate from the new arrangement and the amount of charge carrier on the BSA-covered oxide layer [6,34,54]. Consequently, the total amount of surface potential on the BSA molecule–oxide complex (SP_{surf}) can be defined as [34]:

$$SP_{surf} = SP_{Oxide} + \mu_{BSA}/e + \Delta_{bond} \quad (3)$$

For adsorbed organic layers thicker than 100 nm, the influence of the bulk material normally can be neglected in determining SP_{surf} because of the limited range of interactions between the tip and surface [34,35]. As schematically presented in Fig. 3, some chemical and physical characteristics of the oxide layer and bulk material, such as surface charge, energy, roughness, crystallinity, defects, valance, and conductance states [55], substantially affect electron transfer at the protein/oxide layer interface, which influences the total surface potential response on the adsorbed protein layer.

3.2. Electrochemical analysis at the solid/protein or H_2O_2 interface

As mentioned earlier, the presence of inflammatory cells, particularly macrophages and neutrophils, after insertion of implant materials results in increased concentrations of ROS and H_2O_2. The existence of these highly oxidising chemicals can influence the electrochemical reactions and metal-ion release from the implant surface, and in extreme cases it may result in aseptic loosening of the implant [10,11]. Furthermore, interaction of H_2O_2 with the implant surface can affect the

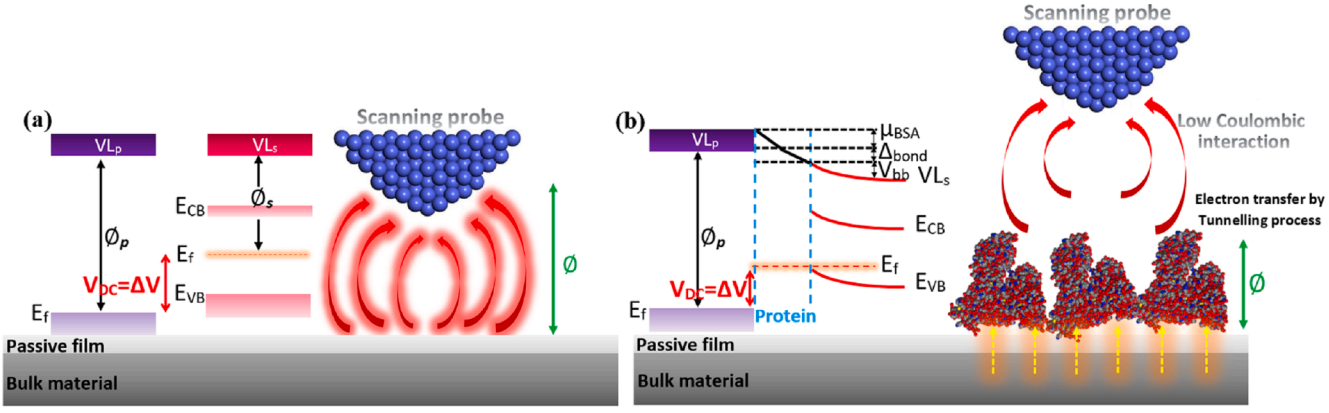

Fig. 1. (a) A schematic representation of SKPFM principle along with energy levels during electrostatic interaction between conductive probe and semiconductor oxide-bulk materials at atomic scale (b) The role of organic adsorbed components (BSA protein) on total surface potential difference.

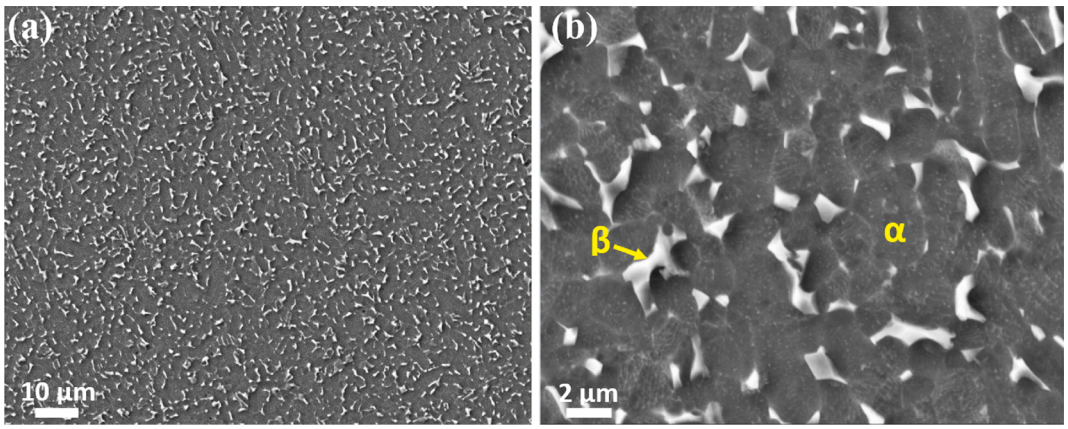

Fig. 2. (a) FE-SEM image of etched Ti6Al4V alloy and (b) high magnification image in (a).

Table 1
WFE calculated from the surface constituent's composition in Ti6Al4V alloy.

Phase	Chemical composition (at%)			Work function energy (WFE, eV)
	Ti	Al	V	
Alpha (α)	86.0	12.0	2.0	4.318 ± 0.004
Beta (β)	79.5	8.3	12.2	4.324 ± 0.008

protein adsorption mechanism on implant materials. In addition, the presence of proteins in the physiological medium and its pre-adsorption on the implant surface can alter the detrimental effect of H_2O_2. In practice, owing to the synergistic effect of inflammatory conditions, the electrochemical potential value of metallic implants, such as CoCrMo, stainless steel, and Ti6Al4V alloys, can shift towards less positive values (e.g. + 500 mV) [12,13,56]. To assess the interplay between H_2O_2 and BSA and their corresponding effect on the electrochemical response of the implant surface, PDP measurements were performed in electrolytes containing only PBS, PBS + H_2O_2, PBS + BSA, or PBS + H_2O_2 + BSA, the results of which are presented in Fig. 4. As can be seen in this figure, the presence of 1 $g{\cdot}L^{-1}$ BSA in the PBS solution decreases the corrosion potential (E_{corr}) by lowering the cathodic reaction branch. It has been previously reported that the BSA can act as a cathodic inhibitor, controlling the cathodic reactions (hydrogen or oxygen evolution) by covering the active sites on the heterogeneous surface with chemisorbed moieties [2,12]. Adsorbed BSA molecules provide conditions for extending the passivity region and increasing the passivity current density (i_{pass}) values on the anodic branch of the PDP curve. This phenomenon can be described based on the BSA–oxide layer interaction in which the protein is the external donor of hydrogen atoms through protonation of its amino acid groups on the oxide layer (e.g. Ti oxide, as seen in reaction (4)), which results in chemisorption of the protein on the surface [57]:

$$Ti-OH+NH_3^+ \rightarrow Ti-OH_2^+ : NH_2-R \quad (4)$$

It is important to note that the phosphate species (e.g. $H_2PO_4^-$ and HPO_4^{2-}) in the PBS solution can also adsorb onto the heterogeneous oxide layer of Ti6Al4V (mainly TiO_2) and in turn trigger the formation of a thin and compact surface film, which reduces the activity or charge transfer through the TiO_2 oxide layer [1,2].

The addition of 100 μM H_2O_2 to the PBS solution strongly affects the electrochemical behaviour. For instance, E_{corr} shifts to more positive values, the passivity region narrows, and i_{pass} increases. H_2O_2 has a high standard electrode potential (1.54 V vs. SCE), and its reduction provides a high positive E_{corr} and high cathodic current densities [11]. Previous studies have indicated that H_2O_2 has a negative impact on the metal ion-release resistance of Ti implant materials by roughening the surfaces and increasing the selective dissolution of the β phase [58–61]. It has also

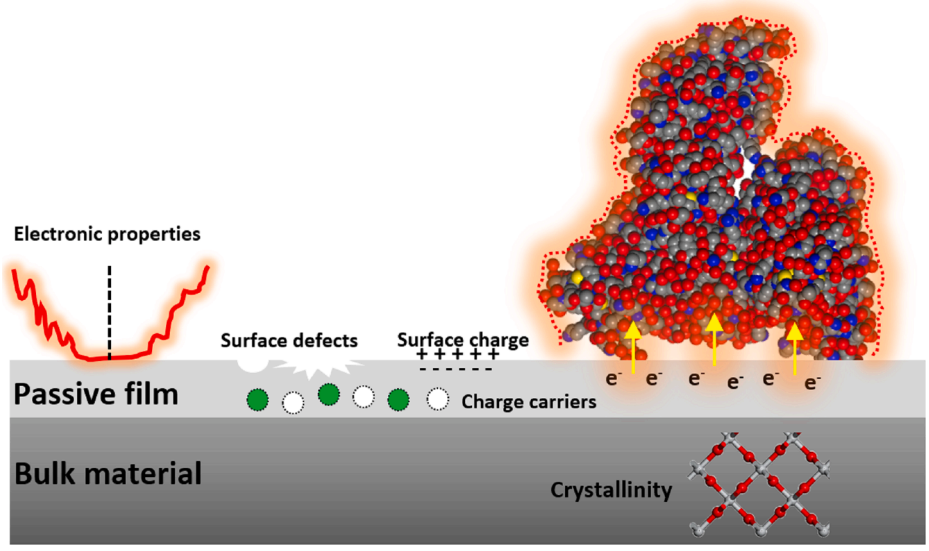

Fig. 3. (a) A schematic representation of some chemical and physical properties of the oxide layer and bulk material which affect the total surface potential of adsorbed proteins layer.

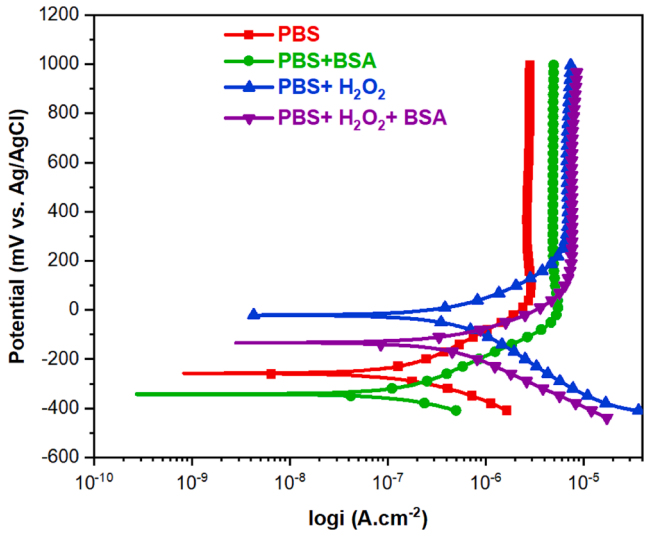

Fig. 4. The PDP curves of Ti6Al4V alloy after 1-hour exposure in PBS, PBS + BSA, PBS + H_2O_2, and PBS + BSA + H_2O_2 environments at 37 °C, pH 7.4, and aerated conditions.

been reported that when Ti is exposed to inflammatory conditions with ROS (e.g. superoxide radical species ($O_2^{\cdot-}$) and H_2O_2) titanium peroxy gel (TiOOH) is formed [62]. Nevertheless, the addition of BSA systems representing harsh inflammatory conditions results in a decrease in E_{corr} and further increase both in the passivity region extention and i_{pass} compared to those in the PBS + H_2O_2 environment. Indeed, BSA adsorption on surface oxides or its complexation with corrosion products on TiO_2 films can damage the protective TiO_2 oxide layer and increase metal ion release due to the metal–protein complex detachment process [3]. Since at + 200 mV vs. Ag/AgCl the Ti6Al4V alloy was in the passive region in all the studied solutions, we anodically polarised the specimens and studied the adsorption of BSA from the solution in the presence and absence of H_2O_2. The presence of adsorbed protein on the surface of the polarised alloy was evaluated by combining SEM, AFM/SKPFM, in-situ AFM, and XPS investigations, as will be discussed in the following section.

3.3. *Influence of H_2O_2 on BSA adsorption, morphology, and surface potential through SKPFM measurements*

Fig. 5 shows SKPFM images at low and high magnifications together with the corresponding SEM images of polished Ti6Al4V samples and samples polarised in PBS, PBS + BSA or PBS + BSA + H_2O_2 solutions, while the topographic AFM images of the same samples are reported in Fig. 6. An SKPFM image of a blank Ti6Al4V surface (Fig. 5**a**) was obtained as a reference surface to recognise the different surface potentials of the α and β phases and to distinguish them after the protein adsorption and surface interactions with H_2O_2. In Fig. 5**b, a** high-resolution surface potential map (obtained from a scanned area of 10 × 10 μm^2) is presented. The α (dark matrix) and β (bright islands) phases in Ti6Al4V are clearly distinguishable because of their different chemical compositions, which results in different *WFE*, as discussed earlier. As can be observed in Fig. 5**a and b**, the absolute surface potential difference between the two phases is sensitive to the size of the scanned area due to inhomogeneity in the chemical composition of the individual phases over a large sample surface area. In Fig. 5**c**, an SEM micrograph of the polished Ti6Al4V sample is provided, in which (except for a few polishing lines) no specific feature can be identified. These polishing lines are also present in Fig. 6**a**. The samples polarised in PBS solution present a very similar surface to that of the fresh sample (Fig. 5**d, e and f**). Nevertheless, a slight decrease of the surface roughness was noticed (Fig. 6**b**), very probably due to the formation of a thicker passive film on the polarized sample.

The SKPFM map of the sample when 1 g·L^{-1} BSA was added to the PBS solution (Fig. 5**g**) is strikingly different from that observed on both the polished surface and polarised in PBS solution. The SKPFM map exhibits a continuous network of dense protein or cluster domains with a lower surface potential than that of the matrix (or oxide layer). Based on the histogram analysis of the surface potential maps in a scanned area of 100 × 100 μm^2 (Fig. 7**b**), the overall surface potential difference (ΔV) on the Ti6Al4V surface in the PBS + BSA condition is slightly lower than that of the polished surface or polarised in PBS solution. This decrease in the surface potential difference reflects that protein adsorption on the surface of Ti6Al4V reduces the heterogeneity of the sample. Moreover, the 1D and 2D PSD analyses presented in Fig. 7**c and d** also show a lower surface potential distribution on the Ti6Al4V surface in the PBS + BSA condition in almost all spatial frequencies. A finer structure composed of round features is also distinguishable in the areas with higher surface potential values (marked with arrows in Fig. 5**g**). A closer examination of the surface potential map obtained from a scanned area of 10 × 10 μm^2 (Fig. 5**h**) shows that even in the presence of adsorbed BSA on the surface, the α and β phases are still distinguishable. However, the amount of adsorbed BSA in the round regions was lower than that on the cluster protein domains, and thus a higher potential was detected. Under polarisation, the heterogeneous surface of the Ti6Al4V alloy (α and β phases) allows BSA to be adsorbed in various ways and exhibit various morphologies [63]. The corresponding SEM micrograph for the sample exposed to PBS + BSA is presented in Fig. 5**i**. In this figure, a continuous network or large clusters of proteins are clearly visible with a dark colour alongside the α and β phases. The observed contrast in the FE-SEM (Fig. 5**i**) image is due to the differences in the electron density of the protein compared to that of the surface oxide. Nevertheless, the fine structure between the protein domains that were detected in the SKPFM maps was not distinguishable owing to the lower sensitivity of the FE-SEM compared to SKPFM for detecting thin layers of organic molecules on the surface. Similar morphologies have been observed for a CoCrMo alloy under cathodic polarisation in PBS + 15 g·L^{-1} BSA at 37 °C [63].

It is important to recognise that the surface potential of proteins and peptides strongly depends on the charge distribution within the polar residues in their structure. Depending on the ionisation state of the main amino acid groups of the protein, a protein may exhibit an overall positive, negative, or neutral charge. The ionisation state of the amino acids within proteins depends on environmental factors, such as the pH of the solution. At the solution pH corresponding to the isoelectric point (IEP), the overall net charge of the protein is zero. At solution pH values above and below the IEP, the overall charge of the protein is negative and positive, respectively [64]. Therefore, the electrostatic interactions between proteins and charged surfaces are greatly influenced by the IEP of the protein [30]. For BSA, the IEP has been determined both theoretically and experimentally to be between 4.7 and 5.4 [6,65]. Therefore, at pH 7 (which was used in this study), the BSA molecules are negatively charged and can strongly interact with the positively charged substrate [42]. As stated above, chemisorption of the BSA molecule on the complexed oxide layer induces new potential steps and band bending in the surface energy levels and reduces the total surface potential (V_{DC}).

The formation of a network-like protein layer, as visualised in Fig. 5**g and h**, is due to protein adsorption on the substrate surface under a mixed adsorption mechanism consisting of Langmuir adsorption and cooperative adsorption mechanisms [66]. In the Langmuir adsorption model, proteins tend to fill the available unoccupied surface sites. Nevertheless, some fluctuations in the density of adsorbed proteins can be expected due to the heterogeneous nature of the oxide layer, which consists of a variety of oxide components [67]. When a sample is polarised to + 200 mV vs. Ag/AgCl (as in this study), the electrostatic attraction between the positively charged oxide layer of the Ti6Al4V sample and negatively charged BSA molecules causes cooperative

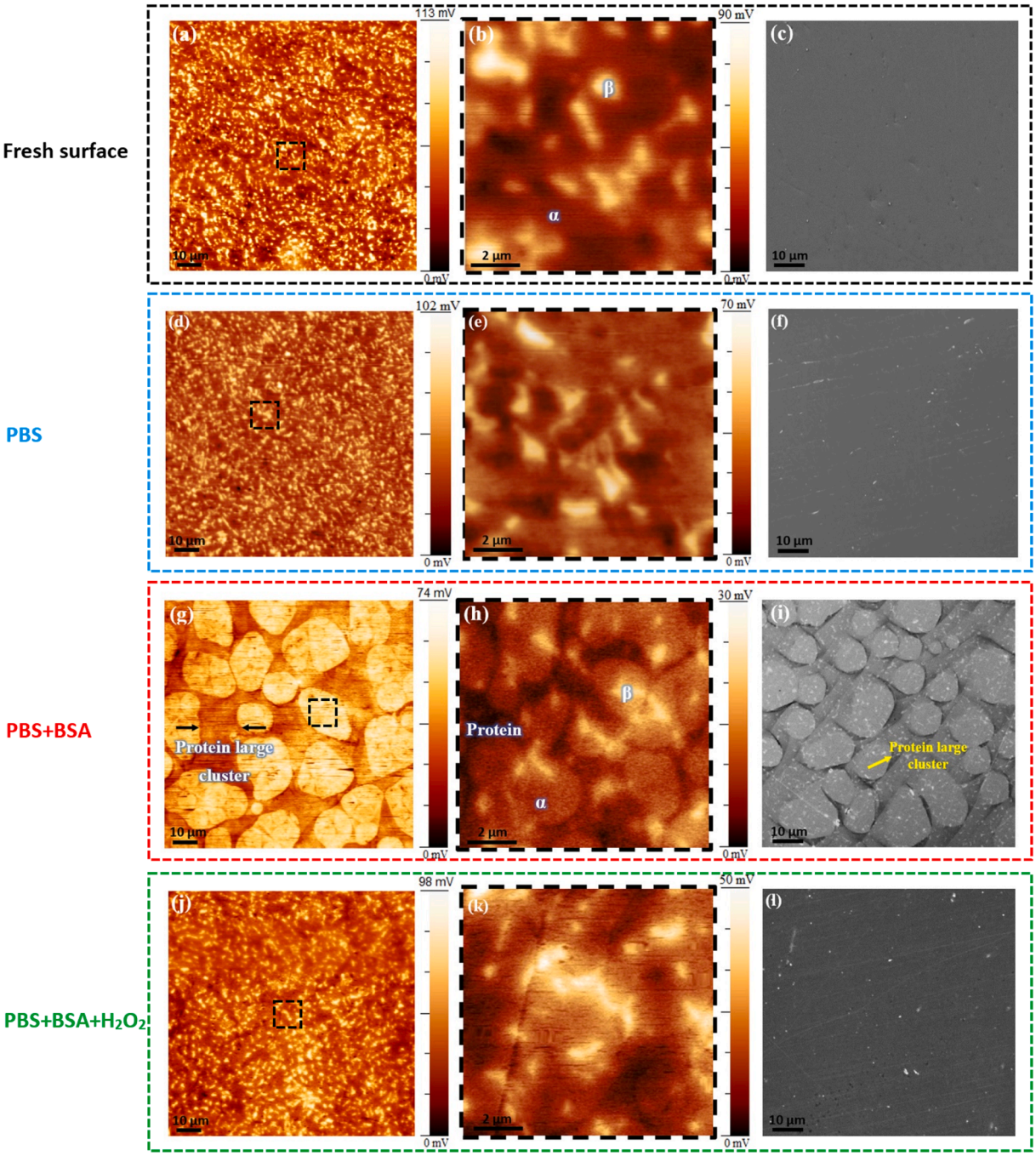

Fig. 5. Sequence images of low and high magnification surface potential maps and FE-SEM image which is correspond to (a, b and c) Ti6Al4V polished or fresh surface, (d, e and f) Ti6Al4V polarised at + 200 mV vs. Ag/AgCl in PBS solution, (g, h and i) Ti6Al4V polarised at + 200 mV vs. Ag/AgCl in PBS + BSA environment, (j, k and l) Ti6Al4V polarised at + 200 mV vs. Ag/AgCl in PBS + BSA + H_2O_2. The polarisation process was carried out for 1-hour at 37 °C and pH 7.4.

adsorption to become the dominant mechanism of protein adsorption [68]. Therefore, the BSA molecules adsorb in the vicinity of pre-adsorbed proteins, which (in combination with the self-migration and lateral movement of the loosely adsorbed proteins) form a network-like morphology and/or cluster domains, as shown in Fig. 5**g** [69]. The cooperative adsorption of proteins on solid substrates has been demonstrated previously using supercritical angle fluorescence microscopy and Monte Carlo simulations [66,70] in systems exhibiting growth of two-dimensional surface clusters that are densely ordered alongside some uncovered regions, which is consistent with the SKPFM result shown in Fig. 5**g**. Consequently, the electrostatic attraction forces at the Ti6Al4V surface/solution–protein interface direct the BSA conformational arrangement into clusters and fine network morphologies, as reported in a previous study [63].

To visualise the presence of the network-like features in solution (similar to those shown in Fig. 5**g and h** in air), we performed complementary in-situ AFM measurements in which the substrate was polarised to + 200 mV vs. Ag/AgCl and BSA was adsorbed onto the surface from the PBS + BSA solution. The result is provided in Fig. 8**,** in which round features between the dense network of adsorbed BSA are clearly visible. The addition of H_2O_2 to the PBS + BSA solution alters the adsorption of proteins on the anodically polarised Ti6Al4V specimen, as presented in the SKPFM map in Fig. 5**j**. As H_2O_2 was introduced into the PBS + BSA solution, the continuous protein network morphology that

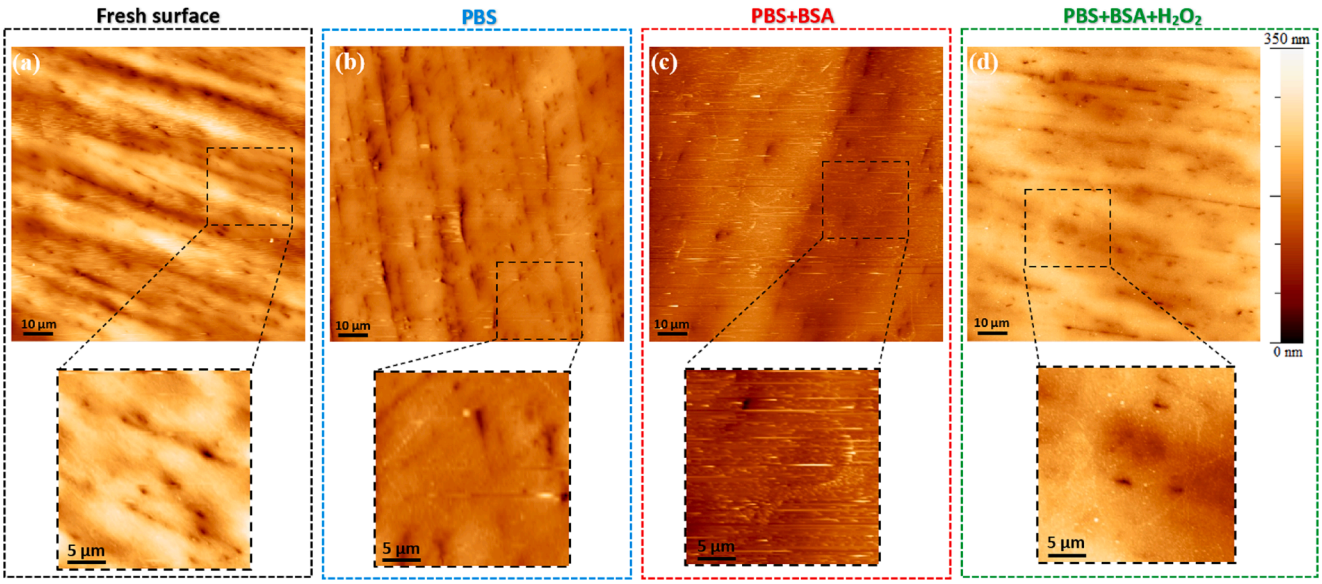

Fig. 6. The topography maps of Ti6Al4V alloy (a) fresh or polished surface, (b) polarised at + 200 mV vs. Ag/AgCl in PBS solution, (c) polarised at + 200 mV vs. Ag/AgCl in PBS + BSA environment (d) polarised at + 200 mV vs. Ag/AgCl in PBS + BSA + H_2O_2, The topography images correspond to the SKPFM images in Fig. 5a, d, g, and j. The polarisation process was carried out for 1-hour at 37 °C and pH 7.4.

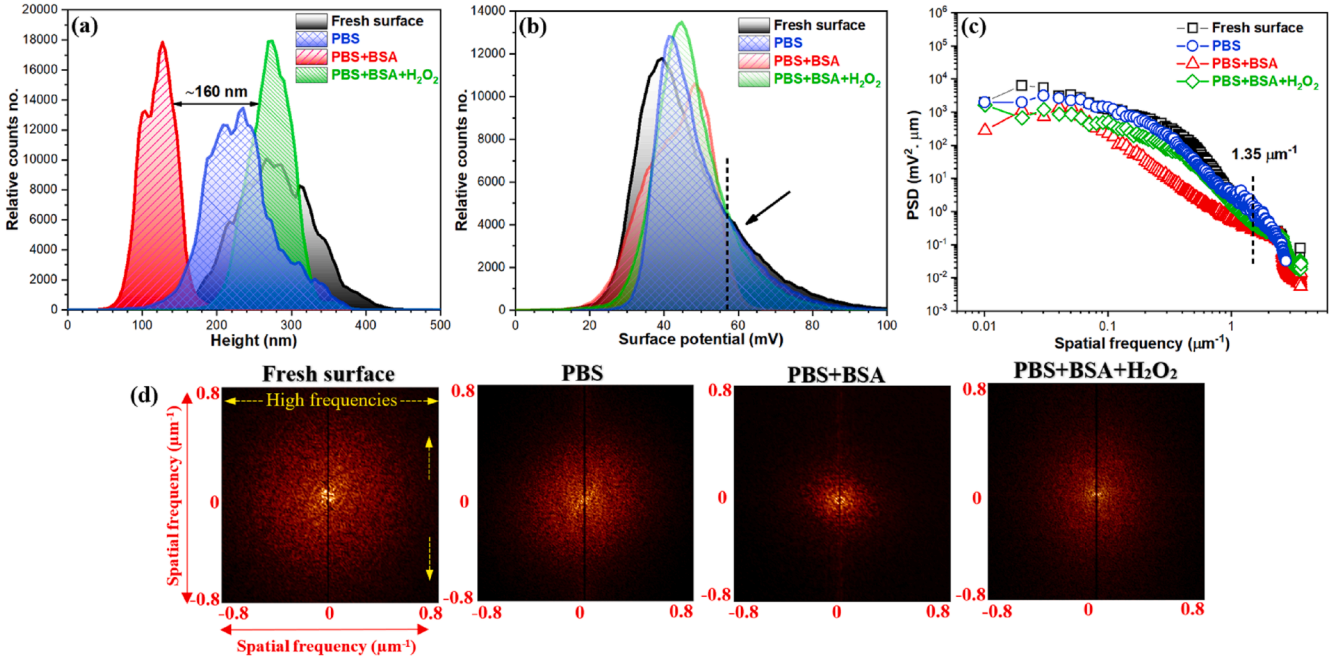

Fig. 7. (a) Topography and (b) surface potential histograms of Ti6Al4V alloy in the different conditions, (c) 1D and (d) 2D PSD analysis. The analyses of (b, c, and d) have been obtained from Fig. 5a, d, g, and j, while the topography histogram analysis in (a) is obtained from Fig. 6.

was observed in the absence of H_2O_2 vanishes completely. The potential contrast observed in Fig. 5**j** in 100 × 100 µm^2 resembles that of the polished sample, indicating that if BSA protein is adsorbed on the surface it does not form large clusters or domains in the presence of H_2O_2. Based on the histogram and PSD analyses in Fig. 7, the surface potential difference in the scanned area of 100 × 100 µm^2 for this sample is lower than that of the polished sample for frequencies lower than 1.35 µm^{-1} (blue arrow in the histogram), confirming the presence of adsorbed proteins on the sample surface, even if clusters have not been observed.

As discussed based on the results in Fig. 5**g and h**, this change in ΔV could potentially indicate that BSA adsorbed onto the Ti6Al4V surface. Furthermore, the high-resolution topography image shown in Fig. 6**d** confirms the presence of protein on the sample surface. Unfortunately, no contrast can be detected in the SEM micrograph shown in Fig. 5**l** because the thickness of the adsorbed protein layer was below the detection limits of FE-SEM. To further confirm the adsorption of BSA on the Ti6Al4V surface from the PBS + BSA + H_2O_2 solution, XPS studies were performed, and the results are presented in Fig. 9. According to previous studies [71,72], the main signal of the C spectrum originates from airborne carbon or surface contamination. Therefore, the C peak on the specimens polarised in PBS and PBS + H_2O_2 solutions can be attributed to contamination. The C 1 s peaks in Fig. 9**a** can be deconvolved into three individual peaks at 284.5 ± 0.9 eV, 285.8 ± 0.8 eV, and 287.7 ± 0.9 eV, which are related to C—C and C—H bonds, peptide

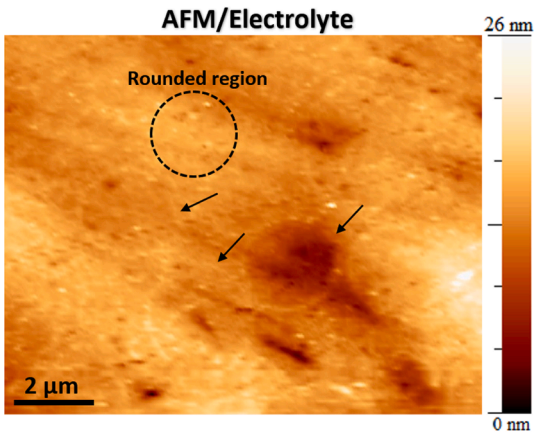

Fig. 8. Topography map (in-situ AFM) of polarised Ti6Al4V samples at + 200 mV vs. Ag/AgCl during 1-hour immersion in PBS + BSA. The measurement has been carried out at 37 °C and pH 7.4, Dashed line and black arrows show the round features formed in the dense network of adsorbed BSA.

residues or C—O and C—N bonds, and N—C═O bonds, respectively [46]. Therefore, it is reasonable to assume that the increase in the intensity of the C and particularly N peaks in the PBS + BSA and PBS + BSA + H_2O_2 conditions was caused by BSA protein adsorption on the Ti6Al4V surface oxide [73]. The BSA protein does not form clusters or domains in presence of H_2O_2 as was mentioned before, but adsorbed rather as a thin film, not detectable with AFM-SKPFM and FE-SEM analyses. Moreover, the two separate peaks in the Ti spectrum at binding energies of 464.8 ± 0.4 eV and 459.1 ± 0.8 eV are attributed to Ti^{4+} $2p_{1/2}$ and T^{i4+} $2p_{3/2}$, respectively, from TiO_2 [46].

Compared to those of the sample exposed to only PBS and PBS + H_2O_2, the intensities of the C 1 s and N 1 s peaks increased, and those of the Ti 2p peaks decreased after the Ti6Al4V specimen was exposed to PBS + BSA + H_2O_2. This clearly confirms the high tendency of BSA protein molecules to adsorb onto the Ti6Al4V surface, a tendency that is slightly enhanced in the presence of H_2O_2 (Fig. 9**c and d)**. In fact, in the presence of both BSA protein and H_2O_2, a slightly higher content of N and a higher content of C are observed on the surface compared to the sample polarised in PBS + BSA solution. However, the amount of Ti does not exhibit big differences when H_2O_2 is added both in the presence and absence of BSA.

It has been reported that the interaction of H_2O_2 with the Ti surface triggers the formation of Ti–H_2O_2 complexes and TiOOH alongside an increase in the surface hydrophilicity and surface roughness [74]. Moreover, according to the histogram analysis of the topography maps in Fig. 7**a**, the surface roughness of the Ti6Al4V surface in the PBS + BSA + H_2O_2 condition shifts to a higher value, approximately 160 nm, compared to that of the specimens polarised in the PBS + BSA solution. It is important to note that the lower surface roughness distribution on the Ti6Al4V surface in both the PBS and PBS + BSA conditions in comparison with that in the PBS + BSA + H_2O_2 condition can be attributed to passive film growth during the application of a positive surface potential as well as the significant role of the covered layer of BSA proteins (only in PBS + BSA). Generally, the inactivation of enzymes, particularly protein fragmentation, can occur in the presence of

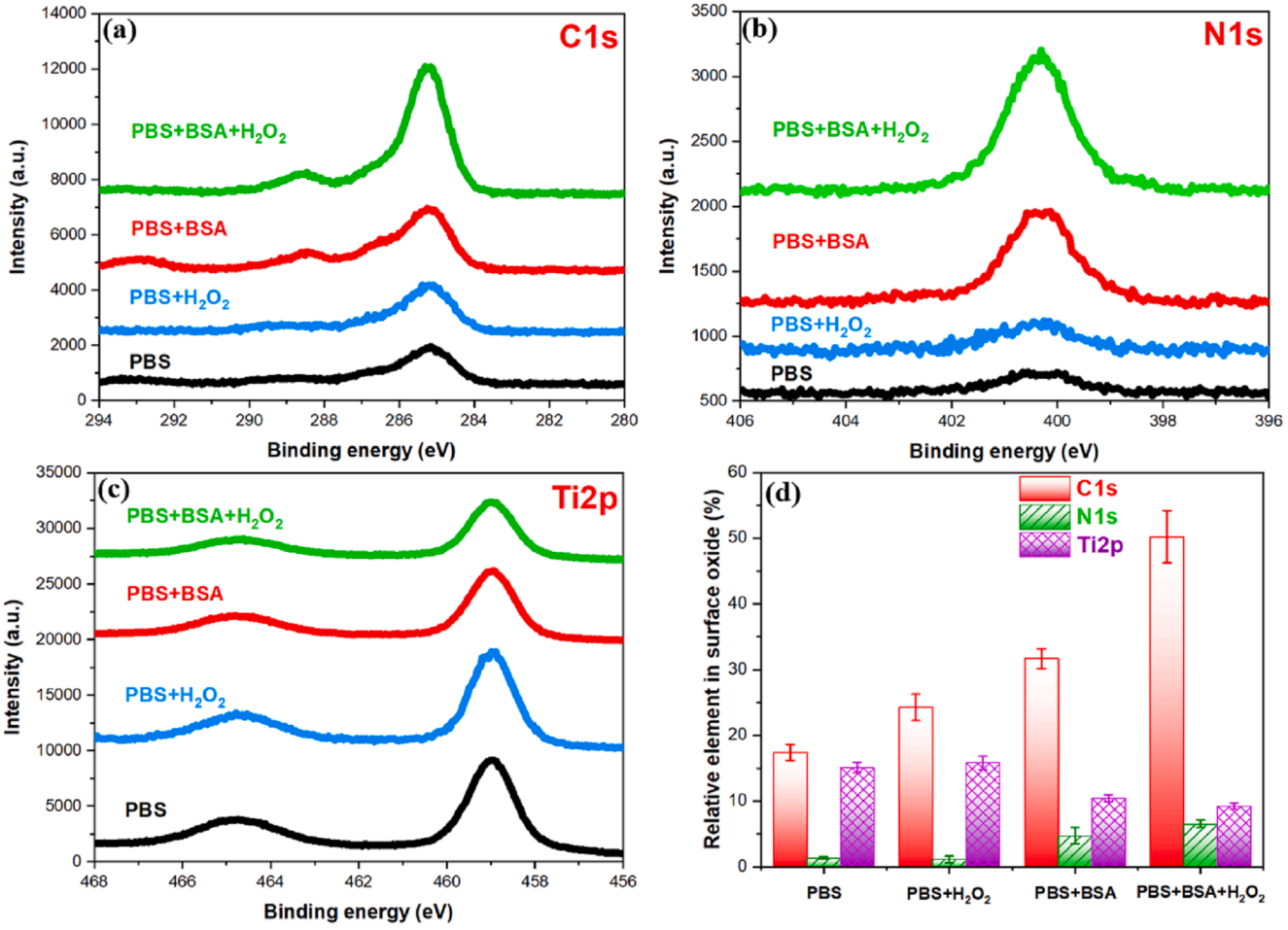

Fig. 9. XPS spectra of (a) C 1 s, (b) N 1 s, and (c) Ti 2p electron energy regions on Ti6Al4V alloy after 1-hour polarisation at + 200 mV vs. Ag/AgCl in PBS, PBS + H_2O_2, PBS + BSA and PBS + BSA + H_2O_2, (d) Relative elements in surface oxide obtained from XPS spectra.

H_2O_2 and $OH^{\cdot}$ scavengers that directly interact with protein and DNA, which damages them [15]. Therefore, H_2O_2 agents can significantly hinder BSA protein molecules from forming the dense protein clusters or a network morphology during the application of a positive potential [14].

4. Conclusion

In this study, SKPFM was utilised as a sensitive method to visualise the impact of H_2O_2 on the adsorption morphology of BSA and the surface potential distribution on the oxide surface of Ti6Al4V alloys in a PBS environment. Based on potentiodynamic polarisation measurements, the H_2O_2 agent in the PBS + BSA + H_2O_2 environment shifts the corrosion potential to substantially more positive values and increases the passivity current in comparison to those in a PBS + BSA medium, thus providing a harsh environment favouring the metal degradation process. By applying a positive surface potential at + 200 mV vs. Ag/AgCl for 1-hour in the passive region of the Ti6Al4V sample during exposure to the PBS + BSA environment, SKPFM and SEM observations identified that the adsorbed BSA forms a dense network morphology or clustering shape. Furthermore, in-situ AFM topography results confirmed the presence of a protein network morphology on the Ti6Al4V sample polarised at + 200 mV vs. Ag/AgCl for 1-hour in the PBS + BSA solution. The very thin protein network morphology that developed in the presence of H_2O_2 did not develop as dense networks or cluster shapes but exhibited a higher total surface potential magnitude in comparison with protein deposition in the absence of H_2O_2. In fact, the protein-covered regions on Ti6Al4V in both PBS + BSA and PBS + BSA + H_2O_2 environments reduces the surface potential compared to that of the uncovered region of the Ti6Al4V matrix with α and β phases. This surface visualisation approach using SKPFM can offer more detailed information about the protein adsorption, conformational arrangement, and surface potential distribution on complex systems in the biomaterials field.

CRediT authorship contribution statement

Ehsan Rahimi: Methodology, Writing - original draft. **Ruben Offoiach:** Methodology, Writing - review & editing. **Saman Hosseinpour:** Methodology, Writing - review & editing. **Ali Davoodi:** Methodology, Writing - review & editing. **Kitty Baert:** Investigation, Methodology. **Alexander Lutz:** Investigation, Methodology. **Herman Terryn:** Writing - review & editing, Resources, Supervision. **Maria Lekka:** Methodology, Writing - review & editing, Resources, Funding acquisition, Supervision, Project administration. **Lorenzo Fedrizzi:** Writing - review & editing, Resources, Supervision.

Declaration of Competing Interest

The authors declare that they have no known competing financial interests or personal relationships that could have appeared to influence the work reported in this paper.

Acknowledgments

This project has received funding from the European Union's Horizon 2020 research and innovation program under the Marie Sklodowska-Curie grant agreement No 764977.

References

[1] M. Talha, Y. Ma, P. Kumar, Y. Lin, A. Singh, Role of protein adsorption in the bio corrosion of metallic implants–A review, Colloids and Surfaces B: Biointerfaces (2019).
[2] I. Milošev, CoCrMo alloy for biomedical applications, Biomedical Applications, Springer, 2012, pp. 1–72.
[3] Y.S. Hedberg, Role of proteins in the degradation of relatively inert alloys in the human body, npj Mater. Degrad. 2 (1) (2018) 26.
[4] P. Roach, D. Farrar, C.C. Perry, Interpretation of protein adsorption: surface-induced conformational changes, J. Am. Chem. Soc. 127 (22) (2005) 8168–8173.
[5] S. Guo, D. Pranantyo, E.-T. Kang, X.J. Loh, X. Zhu, D. Jańczewski, K.G. Neoh, Dominant Albumin-Surface Interactions under Independent Control of Surface Charge and Wettability, Langmuir 34 (5) (2018) 1953–1966.
[6] Y. Yan, H. Yang, Y. Su, L. Qiao, Albumin adsorption on CoCrMo alloy surfaces, Sci. Rep. 5 (2015) 18403.
[7] A. Hasan, V. Saxena, L.M. Pandey, Surface functionalization of Ti6Al4V via self-assembled monolayers for improved protein adsorption and fibroblast adhesion, Langmuir 34 (11) (2018) 3494–3506.
[8] M. Niinomi, Mechanical biocompatibilities of titanium alloys for biomedical applications, J. Mech. Behav. Biomed. Mater. 1 (1) (2008) 30–42.
[9] F. Contu, B. Elsener, H. Böhni, A study of the potentials achieved during mechanical abrasion and the repassivation rate of titanium and Ti6Al4V in inorganic buffer solutions and bovine serum, Electrochim. Acta 50 (1) (2004) 33–41.
[10] R. Tsaryk, M. Kalbacova, U. Hempel, D. Scharnweber, R.E. Unger, P. Dieter, C. J. Kirkpatrick, K. Peters, Response of human endothelial cells to oxidative stress on Ti6Al4V alloy, Biomaterials 28 (5) (2007) 806–813.
[11] F. Yu, O. Addison, A.J. Davenport, A synergistic effect of albumin and H2O2 accelerates corrosion of Ti6Al4V, Acta Biomater. 26 (2015) 355–365.
[12] W. Xu, F. Yu, L. Yang, B. Zhang, B. Hou, Y. Li, Accelerated corrosion of 316L stainless steel in simulated body fluids in the presence of H2O2 and albumin, Mater. Sci. Eng. C 92 (2018) 11–19.
[13] J.-L. Wang, R. Liu, T. Majumdar, S. Mantri, V. Ravi, R. Banerjee, N. Birbilis, A closer look at the in vitro electrochemical characterisation of titanium alloys for biomedical applications using in-situ methods, Acta Biomater. 54 (2017) 469–478.
[14] T. Kocha, M. Yamaguchi, H. Ohtaki, T. Fukuda, T. Aoyagi, Hydrogen peroxide-mediated degradation of protein: different oxidation modes of copper-and iron-dependent hydroxyl radicals on the degradation of albumin, Biochimica et Biophysica Acta (BBA)-Protein Structure and Molecular Enzymology 1337 (2) (1997) 319–326.
[15] M. Roche, P. Rondeau, N.R. Singh, E. Tarnus, E. Bourdon, The antioxidant properties of serum albumin, FEBS Lett. 582 (13) (2008) 1783–1787.
[16] M. Talha, Y. Ma, Y. Lin, A. Singh, W. Liu, X. Kong, Corrosion behaviour of austenitic stainless steels in phosphate buffer saline solution: synergistic effects of protein concentration, time and nitrogen, New J. Chem. 43 (4) (2019) 1943–1955.
[17] I. Ron, L. Sepunaru, S. Itzhakov, T. Belenkova, N. Friedman, I. Pecht, M. Sheves, D. Cahen, Proteins as electronic materials: Electron transport through solid-state protein monolayer junctions, J. Am. Chem. Soc. 132 (12) (2010) 4131–4140.
[18] I. Ron, I. Pecht, M. Sheves, D. Cahen, Proteins as solid-state electronic conductors, Acc. Chem. Res. 43 (7) (2010) 945–953.
[19] A.L. Furst, M.G. Hill, J.K. Barton, A multiplexed, two-electrode platform for biosensing based on DNA-mediated charge transport, Langmuir 31 (23) (2015) 6554–6562.
[20] J. Zhang, A.M. Kuznetsov, I.G. Medvedev, Q. Chi, T. Albrecht, P.S. Jensen, J. Ulstrup, Single-molecule electron transfer in electrochemical environments, Chem. Rev. 108 (7) (2008) 2737–2791.
[21] Q. Chi, O. Farver, J. Ulstrup, Long-range protein electron transfer observed at the single-molecule level: In situ mapping of redox-gated tunneling resonance, Proc. Natl. Acad. Sci. 102 (45) (2005) 16203–16208.
[22] E.A.D. Pia, Q. Chi, D.D. Jones, J.E. Macdonald, J. Ulstrup, M. Elliott, Single-molecule mapping of long-range electron transport for a cytochrome b 562 variant, Nano Lett. 11 (1) (2010) 176–182.
[23] W. Schmickler, N. Tao, Measuring the inverted region of an electron transfer reaction with a scanning tunneling microscope, Electrochim. Acta 42 (18) (1997) 2809–2815.
[24] A. Alessandrini, S. Corni, P. Facci, Unravelling single metalloprotein electron transfer by scanning probe techniques, PCCP 8 (38) (2006) 4383–4397.
[25] V. Palermo, A. Liscio, M. Palma, M. Surin, R. Lazzaroni, P. Samorì, Exploring nanoscale electrical and electronic properties of organic and polymeric functional materials by atomic force microscopy based approaches, Chem. Commun. 32 (2007) 3326–3337.
[26] J.E. Jett, D. Lederman, L.A. Wollenberg, D. Li, D.R. Flora, C.D. Bostick, T.S. Tracy, P.M. Gannett, Measurement of electron transfer through cytochrome P450 protein on nanopillars and the effect of bound substrates, J. Am. Chem. Soc. 135 (10) (2013) 3834–3840.
[27] W. Zhao, W. Cui, S. Xu, L.-Z. Cheong, D. Wang, C. Shen, Direct study of the electrical properties of PC12 cells and hippocampal neurons by EFM and KPFM, Nanoscale Adv. 1 (2) (2019) 537–545.
[28] I. Lee, J.W. Lee, A. Stubna, E. Greenbaum, Measurement of electrostatic potentials above oriented single photosynthetic reaction centers, J. Phys. Chem. B 104 (11) (2000) 2439–2443.
[29] I. Lee, E. Greenbaum, S. Budy, J.R. Hillebrecht, R.R. Birge, J.A. Stuart, Photoinduced surface potential change of bacteriorhodopsin mutant D96N measured by scanning surface potential microscopy, J. Phys. Chem. B 110 (22) (2006) 10982–10990.
[30] A.K. Sinensky, A.M. Belcher, Label-free and high-resolution protein/DNA nanoarray analysis using Kelvin probe force microscopy, nature nanotechnology 2 (10) (2007) 653.
[31] H. Heli, N. Sattarahmady, A. Jabbari, A.A. Moosavi-Movahedi, G.H. Hakimelahi, F.-Y. Tsai, Adsorption of human serum albumin onto glassy carbon surface – Applied to albumin-modified electrode: Mode of protein–ligand interactions, J. Electroanal. Chem. 610 (1) (2007) 67–74.

[32] M.T. Stankovich, A.J. Bard, The electrochemistry of proteins and related substances part III. Bovine serum albumin, J. Electroanal. Chem. Interfacial Electrochem. 86 (1) (1978) 189–199.
[33] D. Xu, G.D. Watt, J.N. Harb, R.C. Davis, Electrical conductivity of ferritin proteins by conductive AFM, Nano Lett. 5 (4) (2005) 571–577.
[34] A. Liscio, V. Palermo, P. Samorì, Nanoscale quantitative measurement of the potential of charged nanostructures by electrostatic and Kelvin probe force microscopy: unraveling electronic processes in complex materials, Acc. Chem. Res. 43 (4) (2010) 541–550.
[35] V. Palermo, M. Palma, P. Samorì, Electronic characterization of organic thin films by Kelvin probe force microscopy, Adv. Mater. 18 (2) (2006) 145–164.
[36] L. Kelvin, V. Contact electricity of metals, The London, Edinburgh, and Dublin Philosophical Magazine and Journal of Science 46(278) (1898) 82–120.
[37] M. Nonnenmacher, M. o'Boyle, H.K. Wickramasinghe, Kelvin probe force microscopy, Appl. Phys. Lett. 58 (25) (1991) 2921–2923.
[38] W. Zisman, A new method of measuring contact potential differences in metals, Rev. Sci. Instrum. 3 (7) (1932) 367–370.
[39] E. Rahimi, A. Kosari, S. Hosseinpour, A. Davoodi, H. Zandbergen, J.M.C. Mol, Characterization of the passive layer on ferrite and austenite phases of super duplex stainless steel, Appl. Surf. Sci. 496 (2019), 143634.
[40] E. Rahimi, A. Rafsanjani-Abbasi, A. Imani, A. Davoodi, TiO2/Cu2O coupled oxide films in Cl− ion containing solution: Volta potential and electronic properties characterization by scanning probe microscopy, Mater. Chem. Phys. 212 (2018) 403–407.
[41] M. Rohwerder, F. Turcu, High-resolution Kelvin probe microscopy in corrosion science: scanning Kelvin probe force microscopy (SKPFM) versus classical scanning Kelvin probe (SKP), Electrochim. Acta 53 (2) (2007) 290–299.
[42] C. Leung, H. Kinns, B.W. Hoogenboom, S. Howorka, P. Mesquida, Imaging surface charges of individual biomolecules, Nano Lett. 9 (7) (2009) 2769–2773.
[43] A. F-06, Standard test method for conducting cyclic potentiodynamic polarization measurements to determine the corrosion susceptibility of small implant devices, ASTM International West Conshohocken, PA, 2001.
[44] B. Halliwell, M.V. Clement, L.H. Long, Hydrogen peroxide in the human body, FEBS Lett. 486 (1) (2000) 10–13.
[45] Z. Esfahani, E. Rahimi, M. Sarvghad, A. Rafsanjani-Abbasi, A. Davoodi, Correlation between the histogram and power spectral density analysis of AFM and SKPFM images in an AA7023/AA5083 FSW joint, J. Alloy. Compd. 744 (2018) 174–181.
[46] E. Rahimi, R. Offoiach, K. Baert, H. Terryn, M. Lekka, L. Fedrizzi, Role of phosphate, calcium species and hydrogen peroxide on albumin protein adsorption on surface oxide of Ti6Al4V alloy, Materialia 15 (2021), 100988.
[47] Z.Q. Liu, W.K. Chim, S.Y. Chiam, J.S. Pan, C.M. Ng, An interface dipole predictive model for high-k dielectric/semiconductor heterostructures using the concept of the dipole neutrality point, J. Mater. Chem. 22 (34) (2012) 17887–17892.
[48] E. Rahimi, A. Rafsanjani-Abbasi, A. Davoodi, S. Hosseinpour, Characterization of the native passive film on ferrite and austenite phases of sensitized 2205 duplex stainless steel, J. Electrochem. Soc. 166 (16) (2019) C609–C616.
[49] H.B. Michaelson, The work function of the elements and its periodicity, J. Appl. Phys. 48 (11) (1977) 4729–4733.
[50] M.T. Greiner, M.G. Helander, W.-M. Tang, Z.-B. Wang, J. Qiu, Z.-H. Lu, Universal energy-level alignment of molecules on metal oxides, Nat. Mater. 11 (1) (2012) 76.
[51] P. Silva-Bermudez, S. Rodil, An overview of protein adsorption on metal oxide coatings for biomedical implants, Surf. Coat. Technol. 233 (2013) 147–158.
[52] Á. Dávila-Grana, L. Diego-González, Á. González-Fernández, R. Simón-Vázquez, Synergistic Effect of Metal Oxide Nanoparticles on Cell Viability and Activation of MAP Kinases and NFκB, Int. J. Mol. Sci. 19 (1) (2018) 246.
[53] J. Lü, E. Delamarche, L. Eng, R. Bennewitz, E. Meyer, H.-J. Güntherodt, Kelvin probe force microscopy on surfaces: Investigation of the surface potential of self-assembled monolayers on gold, Langmuir 15 (23) (1999) 8184–8188.
[54] Z. Zhang, J.T. Yates Jr, Band bending in semiconductors: chemical and physical consequences at surfaces and interfaces, Chem. Rev. 112 (10) (2012) 5520–5551.
[55] A.E. Nel, L. Mädler, D. Velegol, T. Xia, E.M. Hoek, P. Somasundaran, F. Klaessig, V. Castranova, M. Thompson, Understanding biophysicochemical interactions at the nano–bio interface, Nat. Mater. 8 (7) (2009) 543–557.
[56] Y. Liu, J.L. Gilbert, Effect of simulated inflammatory conditions and potential on dissolution and surface oxide of CoCrMo alloy: In situ electrochemical atomic force microscopy study, Electrochim. Acta 262 (2018) 252–263.
[57] S. Karimi, A. Alfantazi, Electrochemical corrosion behavior of orthopedic biomaterials in presence of human serum albumin, J. Electrochem. Soc. 160 (6) (2013) C206–C214.
[58] J. Pan, D. Thierry, C. Leygraf, Electrochemical impedance spectroscopy study of the passive oxide film on titanium for implant application, Electrochim. Acta 41 (7–8) (1996) 1143–1153.
[59] J. Pan, D. Thierry, C. Leygraf, Hydrogen peroxide toward enhanced oxide growth on titanium in PBS solution: blue coloration and clinical relevance, Journal of Biomedical Materials Research: An Official Journal of The Society for Biomaterials and The Japanese Society for, Biomaterials 30 (3) (1996) 393–402.
[60] C. Fonseca, M. Barbosa, Corrosion behaviour of titanium in biofluids containing H2O2 studied by electrochemical impedance spectroscopy, Corros. Sci. 43 (3) (2001) 547–559.
[61] Y. Zhang, O. Addison, F. Yu, B.C.R. Troconis, J.R. Scully, A.J. Davenport, Time-dependent enhanced corrosion of Ti6Al4V in the presence of H 2 O 2 and albumin, Sci. Rep. 8 (1) (2018) 3185.
[62] P. Tengvall, H. Elwing, I. Lundström, Titanium gel made from metallic titanium and hydrogen peroxide, J. Colloid Interface Sci. 130 (2) (1989) 405–413.
[63] R. Namus, J. Nutter, J. Qi, W.M. Rainforth, The influence of protein concentration, temperature and cathodic polarization on the surface status of CoCrMo biomedical grade alloys, Appl. Surf. Sci. 499 (2020), 143908.
[64] K. Rezwan, L.P. Meier, M. Rezwan, J. Vörös, M. Textor, L.J. Gauckler, Bovine serum albumin adsorption onto colloidal Al2O3 particles: a new model based on zeta potential and UV− Vis measurements, Langmuir 20 (23) (2004) 10055–10061.
[65] T. Guckeisen, S. Hosseinpour, W. Peukert, Isoelectric points of proteins at the air/liquid interface and in solution, Langmuir (2019).
[66] A.P. Minton, Effects of excluded surface area and adsorbate clustering on surface adsorption of proteins. II. kinetic models, Biophys. J. 80 (4) (2001) 1641–1648.
[67] M. Rabe, D. Verdes, S. Seeger, Understanding cooperative protein adsorption events at the microscopic scale: a comparison between experimental data and Monte Carlo simulations, J. Phys. Chem. B 114 (17) (2010) 5862–5869.
[68] M. Rabe, D. Verdes, J. Zimmermann, S. Seeger, Surface organization and cooperativity during nonspecific protein adsorption events, J. Phys. Chem. B 112 (44) (2008) 13971–13980.
[69] H. Min, E. Freeman, W. Zhang, C. Ashraf, D. Allara, A.C. Van Duin, S. Tadigadapa, Modified random sequential adsorption model for understanding kinetics of proteins adsorption at a liquid-solid interface, Langmuir 33 (29) (2017) 7215–7224.
[70] M. Rabe, D. Verdes, S. Seeger, Understanding protein adsorption phenomena at solid surfaces, Adv. Colloid Interface Sci. 162 (1–2) (2011) 87–106.
[71] S. Karimi, T. Nickchi, A. Alfantazi, Effects of bovine serum albumin on the corrosion behaviour of AISI 316L, Co–28Cr–6Mo, and Ti–6Al–4V alloys in phosphate buffered saline solutions, Corros. Sci. 53 (10) (2011) 3262–3272.
[72] S. Karimi, T. Nickchi, A.M. Alfantazi, Long-term corrosion investigation of AISI 316L, Co–28Cr–6Mo, and Ti–6Al–4V alloys in simulated body solutions, Appl. Surf. Sci. 258 (16) (2012) 6087–6096.
[73] Y.S. Hedberg, M. Žnidaršič, G. Herting, I. Milošev, I. Odnevall Wallinder, Mechanistic insight on the combined effect of albumin and hydrogen peroxide on surface oxide composition and extent of metal release from Ti6Al4V, Journal of Biomedical Materials Research Part B: Applied, Biomaterials 107 (3) (2019) 858–867.
[74] M. Nagassa, A. Daw, W.G. Rowe, A. Carley, D.W. Thomas, R. Moseley, Optimisation of the hydrogen peroxide pre-treatment of titanium: surface characterisation and protein adsorption, Clin. Oral Implant. Res. 19 (12) (2008) 1317–1326.